THE JOURNAL OF PHYSICAL CHEMISTRY C

Article

pubs.acs.org/JPCC

Evidence for the Predominance of Condensed Phase Reaction in Chemical Looping Reactions between Carbon and Oxygen Carriers

Nicholas W. Piekiel, Garth C. Egan, Kyle T. Sullivan, and Michael R. Zachariah*

Department of Mechanical Engineering and Department of Chemistry and Biochemistry, University of Maryland, College Park, Maryland, 20742 United States

ABSTRACT: This study investigates the use of metal oxides as an oxygen carrier in chemical looping combustion applications. The initiation and decomposition of C/CuO and C/Fe_2O_3 are investigated using a time-resolved T-jump/time-of-flight mass spectrometer (T-Jump/TOFMS). Heating of the metal oxide nanopowders produces gaseous O_2, but when mixed with the fuel (carbon), gaseous O_2 forms temporally after the primary combustion product, CO_2. This indicates condensed phase reaction between the metal oxide and carbon as the predominant reaction mechanism rather than gas phase release of O_2 and subsequent burning of carbon, at least in the initiation phase. In situ heating TEM, and SEM are used to further investigate the reaction. The oxidation rate of carbon in the present experiment is estimated to be 3 to 5 orders of magnitude greater than that predicted using the Nagle Strickland-Constable model. The activation energy of C/CuO, C/Fe_2O_3, and C/Bi_2O_3 are determined using the Ozawa iso-conversion method and are found to be 110, 170, and 230 kJ/mol, respectively. The condensed phase nature of this reaction is compared to our previous studies on aluminum nanothermites and is considered to be further evidence toward a reactive sintering initiation mechanism.

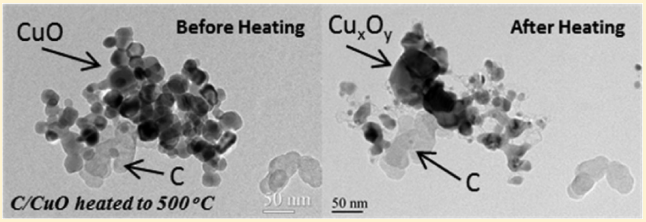

INTRODUCTION

Carbon combustion remains a primary energy source for meeting the world's current and future energy demands. However, CO_2 production during combustion remains a critical issue. Carbon sequestration is one method to prevent CO_2 release, but this process generally has significant monetary and energy use concerns. Chemical looping combustion (CLC) was originally conceived as a method to increase the thermal efficiency of power generation stations but was later recognized for its CO_2 sequestration capability for combustion of coal and other heavy hydrocarbon sources, with minimal energy penalty.[1] By employing metal oxides as the oxygen carrier there is potential for CO_2 as the only gas phase reaction product (with air as the oxidizer N_2 gas and other nitrogen containing species are prominent), enabling easier sequestration.

The majority of CLC studies use a fluidized bed reactor, flowing syngas over an oxidizing agent made up of neat metal oxide particles or a metal oxide/inert support system.[2−5] These experiments tend to focus on implementation of a CLC system and reproducibility of the oxygenation and reduction processes. A few studies also examine direct oxygenation of the fuel by metal oxides.[6,7] Siriwardane and co-workers investigated the reaction mechanism of CuO and carbon particles and found significant differences in the reaction when the two materials are in contact, compared to when they are separated by a small gap. With the materials in contact, a low temperature mechanism is observed, where C and CuO react through a condensed phase reaction between 673 and 873 K. They suggest that the surface of the CuO, which has a Tammann temperature of ∼678 K, melts and provides a pathway for oxygen distribution to the solid coal.[7] [The Tammann temperature is usually considered as half of the bulk melting point of a material. This is the temperature at which surface atoms begin to gain a significant amount of mobility.[8]] The use of this low temperature reaction may result in a more efficient process if a lower energy input is required to sustain combustion. To improve this method even further, more must be known about the mechanism of reaction between the fuel and oxidizer.

A mixture of carbon and metal oxide particles is physically similar to a mixture of aluminum and metal oxide particles and may share mechanistic properties, that we take into account when considering the carbon reaction. However, as with the chemical looping process, most thermite studies fail to probe the oxygen delivery mechanism to the aluminum fuel, and this process remains unclear. The correlation of nanothermite ignition with gaseous oxygen release from the metal oxide has been previously highlighted.[9] While there is a clear trend between these two events it is still not conclusive that the mechanism is a heterogeneous reaction between the condensed phase aluminum and gaseous oxidizer.

Several previous experiments within our group have suggested a condensed phase reaction mechanism for aluminum with metal oxide particles. Our recent study on Al/Bi_2O_3 shows ignition at a temperature well below that where

Received: April 30, 2012
Revised: August 30, 2012
Published: October 4, 2012

gas phase O_2 is released from Bi_2O_3.[10] Since the system is reacting without the presence of a gas phase oxidizer, this suggests that there is condensed phase chemistry occurring. We also performed a high heating rate SEM study, which allowed for in situ heating of aluminum/metal oxide mixtures and imaging before and after heating.[11] The system was used with an Al/WO_3 nanocomposite that demonstrated significant morphological changes after heating of fuel and oxidizer particles that were in physical contact. Particles that were not in contact demonstrated little to no morphological changes after heating. From this study we proposed a "reactive sintering" model to explain the initiation of nanothermite reactions. This model predicts that when the fuel and oxidizer are in intimate contact, a low temperature exothermic reaction occurs. This promotes further sintering of the reactants, resulting in an increase of the effective surface area, facilitating a more rapid reaction. However, due to the relatively low melting point of aluminum in each of these studies, the mechanism becomes complex and it is not clear whether this reaction requires aluminum to be in the liquid phase.

With carbon as a fuel, the reaction will be governed by oxide transport to the carbon, since carbon will remain in the solid phase within the temperature regime of T-Jump heating experiments (unlike an aluminum fuel). The question is whether the oxygen carrier liberates the oxygen to the gas phase or alternatively transports the oxygen to the fuel in the condensed phase. During a rapid heating SEM study of sparsely placed aluminum and bismuth oxide particles atop a carbon film, further evidence for condensed phase reaction was observed as the bismuth oxide particles reacted with the underlying carbon film, rather than the nearby aluminum.[10] This was further investigated using the temperature-jump/time-of-flight mass spectrometer (T-Jump/TOFMS) and a C/Bi_2O_3 mixture, for which a condensed phase reaction was also observed. However, Bi_2O_3 is a unique oxidizer in that it changes crystalline phase to δ-Bi_2O_3 shortly before melting and becomes a very efficient oxide ion conductor.[12] This means that Bi_2O_3 effectively transports and produces oxygen ions throughout its condensed lattice, making it an oxygen producer and conductor in the condensed phase.[12] While Bi_2O_3 is clearly a unique material, there are limited studies that suggest other metal oxides such as CuO and Fe_2O_3 possess similar properties.[7,13,14]

Again, most work on soot oxidation or CLC assumes a gaseous oxidizing environment, but some of these studies have contributed significantly to the understanding of the kinetics of carbon oxidation. Previous soot oxidation experiments include, but are not limited to, shock tube studies on soot aerosols,[15,16] thermogravimetric analysis of soot nanoparticles,[17] optical analysis of heated carbon rods,[18] and flow reactors paired with nondispersive infrared detection[19] or tandem differential mobility characterization.[20] The Nagle and Strickland-Constable (NSC) model, which is outlined by Walls and Strickland-Constable,[18] is frequently used to predict the rate of oxidation for carbon and soot particles. When compared with experimental results, this model provides varying degrees of correlation. At high temperatures, Park and co-workers observed oxidation rates that were a factor of 2 greater than predicted by the NSC model,[16] Gilot et al. observed slower oxidation rates,[17] whereas Higgins et al. obtained a good correlation with the NSC model.[20]

The focus of the present study is on characterizing the reaction in carbon/metal oxide mixtures. The concentration profiles of gas phase products are analyzed to investigate the initiation events, and TEM and SEM studies are used to observe changes in particle morphology. Varied heating rate experiments are also performed to determine the activation energy for the carbon/metal oxide reactions.

EXPERIMENTAL SECTION

The main experimental tool is a T-Jump/TOFMS, which is described in detail elsewhere.[9,21] This system consists of a disposable fine platinum filament (1−2 cm length, 76 μm diameter) that serves as the heating surface for this experiment and can reach heating rates of up to $\sim 6 \times 10^5$ K/s. The temperature of the filament is determined by simultaneously recording the current and voltage across the filament and calculating the change in resistivity of the platinum during heating. The resistivity can then be related to the temperature of the filament by the Callendar−Van Dusen equation.[22] Previous experiments suggest that there is little temperature gradient along the length of the wire due to the fast rate of heating and relatively slow rate of conductive heat loss. In order to rapidly sample the reaction products, the filament is placed ~1 cm away from the ionization region of the mass spectrometer. As the sample is heated the reaction products quickly travel from the wire to the 70 eV electron beam ionization source. The electron beam is directed between two pulsed, high-voltage plates that are used to accelerate the ions through the TOF tube to a microchannel plate (MCP) detector. In a typical experimental run, sampling takes place for 9.5 ms while the high voltage plates are pulsed at 10,000 Hz, producing a spectrum every 100 μs.

All samples are stoichiometrically mixed in-house following the reaction

$$C + MO \rightarrow CO_2 + M \quad (1)$$

where the carbon and metal oxides are commercially available nanopowders. The carbon used in this study is "regal 300" from Cabot Corporation (<50 nm), and the metal oxides, CuO (<50 nm), Fe_2O_3 (<50 nm), and Bi_2O_3 (90−210 nm), are from Sigma Aldrich with primary particle sizes listed by the supplier. Samples are placed in hexane and ultra-sonicated for ~20 min in order to ensure intimate mixing of the particles. A micropipet is used to apply the sample solution to the platinum filament. After application of the sample and prior to the start of the heating pulse, the filament is placed in vacuum and allowed to dry for ~5 min.

Varied heating rate experiments were used to determine the activation energy of the carbon/metal oxide reaction. The C/CuO, C/Fe_2O_3, and C/Bi_2O_3 mixtures were heated at four separate heating rates ranging from 45 000 to 550 000 K/s, and four data points were recorded at each heating rate. The Ozawa isoconversion method[23]

$$\ln(\beta_i) = \text{constant} - \frac{1.05E_a}{RT_{a,i}} \quad (2)$$

was used to determine the activation energy, where β is the heating rate, E_a is the activation energy, T_a is the temperature at a given point of the reaction, and R is the universal gas constant.[24] For each data point, the reported temperature is that of the filament at the first detection of CO_2 by our mass spectrometer. This value is a constant point of conversion at each heating rate, which is necessary for the Ozawa method. For kinetic analysis using the Ozawa method it is desirable to analyze the activation energy over the entire reaction as the

dx.doi.org/10.1021/jp304148c | J. Phys. Chem. C 2012, 116, 24496−24502

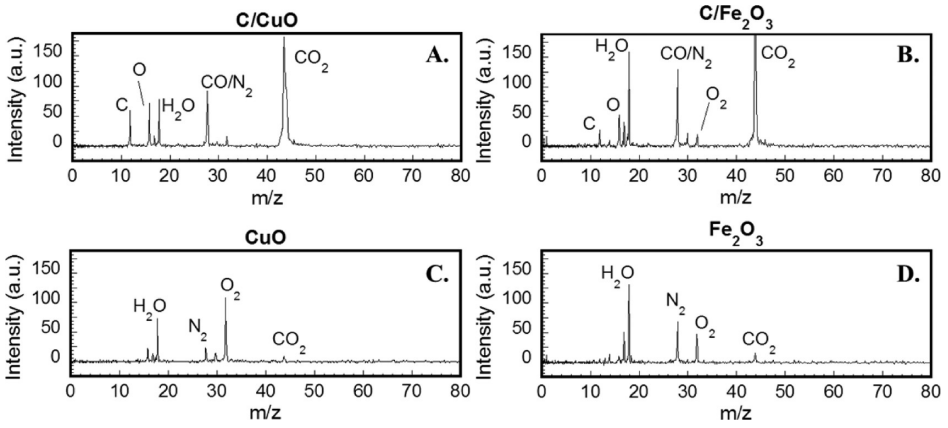

Figure 1. Individual mass spectra during rapid heating in T-Jump/TOF experiments of (a) C/CuO, (b) C/Fe_2O_3, (c) CuO, and (d) Fe_2O_3. Each spectrum was obtained shortly after initiation of the reaction, and shows all representative species of the reaction.

value may vary at different extents of reaction.[24] This type of evaluation is not currently possible with the T-Jump/TOFMS. However, the experimental conditions of this system allow for kinetic analysis at heating rates that are orders of magnitude faster than typically used, and can therefore provide an interesting look at the initial reaction.

Transmission electron microscopy (TEM) and scanning electron microscopy (SEM) were used to observe particle morphology at different stages of reaction. The TEM system was used with in situ heating at a rate of ~500 K/min up to a temperature of 723 K and then held at constant temperature for 2−3 min before cooling. Images were taken prior to and after heating to observe the changes near the onset reaction temperature. For the SEM study, a mixture of carbon and CuO particles were rapidly heated on the platinum wire at ~5 × 10^5 K/s to observe morphological changes under high heating rates. Energy dispersive X-ray spectroscopy (EDS) was used for elemental analysis of the condensed reaction products on the platinum wire.

RESULTS AND DISCUSSION

To investigate the reaction products from rapid heating of carbon/metal oxide mixtures, the neat metal oxides and mixtures were individually heated in separate experimental runs. Preliminary investigation of C/Bi_2O_3 has been performed[10] to complement a study on Al/Bi_2O_3. This investigation focused on the initial condensed phase reaction between carbon and bismuth oxide but did not expand into further details on the reaction. Further analysis on this reaction is provided below, but the primary focus is given to C/CuO and C/Fe_2O_3. Figure 1a−d shows individual detailed spectra for C/CuO, C/Fe_2O_3, and the neat oxide nanopowders CuO and Fe_2O_3, respectively. A typical background spectrum for the mass spectrometer consists of a large peak at mass to charge ratio (m/z) 18 (H_2O) and smaller peaks at m/z 28 (N_2), m/z 32 (O_2), and m/z 17 (OH), which results from fragmentation of H_2O during ionization. The main reaction product for the carbon/metal oxide combustion in vacuum is CO_2 (m/z 44) as can be seen in both Figure 1a,b, which corresponds to previous studies on C/Bi_2O_3.[10] There are several smaller peaks observed at m/z 12 (C) and 16 (O) as well as an increase in m/z 28 (CO). These are all considered to be due to fragmentation of the CO_2 molecule during ionization and follows what is reported for the CO_2 mass spectrum in the NIST spectral library.[25] The small peak at m/z 32 (O_2) is due to excess oxygen that is released to the gas phase. For the neat nanopowders, there is a significant difference in the amount of CO_2 and O_2 as compared to the fuel/oxide mixtures. In both panels c and d in Figure 1, the intensity of O_2 is greater than that in the mixtures, and the CO_2 is substantially decreased. Comparison of the fuel/oxide vs neat oxide nanopowders shows that the O_2 formed by the metal oxides is almost entirely consumed to form CO_2. Although no carbon is added to the neat oxide nanopowders, some CO_2 production is observed. This CO_2 production is presumably due to a reaction between the metal oxide and a small amount of residual carbon leftover from the hexane solvent.

Although carbon dioxide is identified as the prominent gaseous product species, the sequence of the reaction processes is still unclear. To further investigate the reaction pathway, comparison is made between time-resolved profiles of the detected product species for the neat metal oxide nanopowders and the fuel/oxide mixtures. The molecular oxygen release profile from the neat CuO is compared with the carbon dioxide release from C/CuO in Figure 2. This gives a correlation between the time (which corresponds to filament temperature) that the O_2 is released from the oxide and when the reaction starts to progress in C/CuO. Although the traces in Figure 2 are from different experimental runs, similar heating pulses and wire lengths were used so that comparison between runs can be

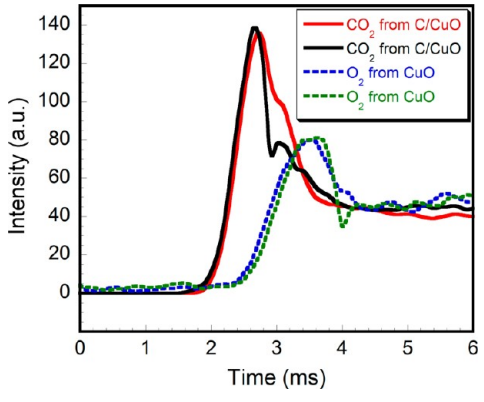

Figure 2. Detected product concentrations for CO_2 from C/CuO and O_2 from CuO. A total of four runs are shown: two for C/CuO and two for CuO. Each experimental run was performed under similar heating conditions. O_2 signals have been zeroed to compensate for the background O_2 signal.

dx.doi.org/10.1021/jp304148c | J. Phys. Chem. C 2012, 116, 24496−24502

confidently made. As an example of the repeatability of these events, a total of four separate heating experiments are shown in Figure 2; two for neat copper oxide heating and two for carbon/copper oxide. From Figure 2 it can be seen that the onset of CO_2 as produced from the C/CuO occurs at a lower temperature than O_2 release from CuO. This strongly implies that there is a condensed phase reaction mechanism driving the CO_2 producing reaction. Figure 3 is similar to Figure 2 but

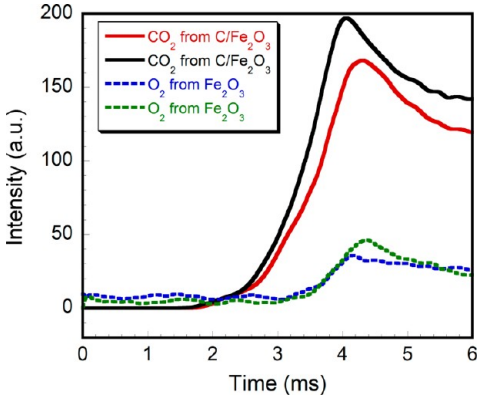

Figure 3. Detected product concentrations for CO_2 from C/Fe_2O_3 and O_2 from Fe_2O_3. A total of four runs are shown: two for C/Fe_2O_3 and two for Fe_2O_3. Each experimental run was performed under similar heating conditions. O_2 signals have been zeroed to compensate for the background O_2 signal.

plots the CO_2 production from C/Fe_2O_3 along with the O_2 release from Fe_2O_3. This figure shows the same trend as that for C/CuO; that is, carbon dioxide is produced well before a gaseous oxidizer is available; therefore, the initiation of this reaction must also be in the condensed phase. This conclusion matches what was observed for the reaction between C/Bi_2O_3.[10]

A calculation was performed to quantify the rate of carbon oxidation using parameters obtained from the T-Jump/TOFMS experiments. In predicting the reaction rate from the experiments, parameters that require estimation such as mass and reaction time were conservatively chosen to avoid bias toward the results. To determine the reaction rate from our experiment, we consider the oxidation of one carbon nanoparticle within the time scale of the experiment. Assuming a 50 nm carbon particle (mass of $\sim 1.3 \times 10^{-16}$ g) where the reaction occurs at the surface in a time of ~0.9 ms (average rise time for CO_2 production from C/Fe_2O_3), we obtain a reaction rate estimation of ~0.007 g cm^{-2} s^{-1} for C/Fe_2O_3, ~0.01 g cm^{-2} s^{-1} for C/CuO (reaction time of ~0.6 ms), and ~0.02 g cm^{-2} s^{-1} for C/Bi_2O_3 (reaction time of ~0.4 ms).

The assumptions made from the mass spectra can only be used to analyze the reaction rate if the reaction progresses to completion within the time scale of the rapid heating events. To investigate the extent of reaction, SEM images were taken of the condensed phase reaction products after rapid heating on the platinum filament, and are shown in Figure 4. From these images, various stages of reaction can be observed on the filament. Elemental analysis was performed in two sections of the wire with varying degrees of reaction, as indicated in Figure 4. The summary of elemental analysis for each section is listed in Table 1.

Comparing points A and B of Figure 4 and the data in Table 1, the reaction has progressed much further in the region of

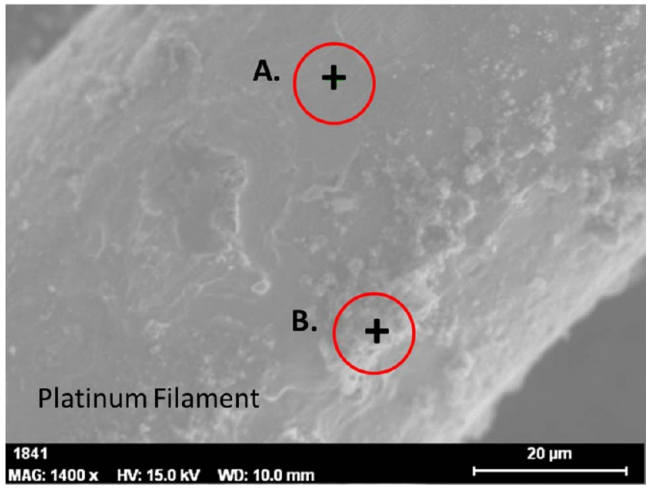

Figure 4. SEM image of the condensed phase reaction products of C/CuO on a platinum filament after heating at $\sim 5 \times 10^5$ K s^{-1}. A and B denote the points where EDS was performed.

Table 1. Summary of EDS Analysis for the Points A and B Shown in Figure 4

	wt %	
element	point A	point B
C	5.78	43.50
Cu	58.74	40.42
Pt	33.65	7.22
O	2.10	8.86

point A than in that of point B. The variance in reaction is due to heat transfer through the layers of carbon/copper oxide powder. The layers that are near to, or touching the platinum filament will follow the temperature of the filament closely. Particles that are off of the filament will be at a significantly lower temperature and therefore, are more likely to undergo a lower extent of reaction. The spectra obtained during rapid heating are representative of the initial reaction events or the reactions between particles whose temperature follows that of the filament. It can be seen from the elemental analysis of point A of Figure 4 that these particles undergo a near complete reaction, and thus, our assumptions based on the spectra are valid.

To compare these predicted reaction rates with traditional carbon oxidation studies, the NSC model is used as applied by Park and Appleton,[16] for which the equations are listed in Appendix A. These calculations were performed for C/CuO, C/Fe_2O_3, and C/Bi_2O_3 at the respective initiation temperature from T-Jump/TOFMS at the highest heating rate (temperatures are shown in Figure 5). The values for the reaction rate and initiation temperature for each fuel/oxide system are given in Table 2. For each system, the reaction rate predicted by the NSC model is at least 4 orders of magnitude slower than the experimental reaction rates. The higher reaction rate as determined from the experiment implies that the metal oxide proximity and nature of contact with the fuel will play a significant role. The condensed phase transport processes may also serve to enhance the diffusion of the oxidizer to increase the overall reaction rate.

It is possible that some error exists in the NSC calculation as the two input parameters, temperature and pressure represent sources of uncertainty. For the C/Fe_2O_3, which undergoes an

dx.doi.org/10.1021/jp304148c | J. Phys. Chem. C 2012, 116, 24496−24502

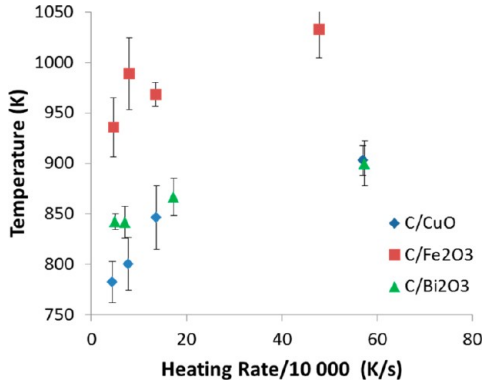

Figure 5. Decomposition temperatures taken from the onset of CO_2 production at various heating rates Each point is an averaged value from 4 experimental runs. Error bars represent the standard deviation.

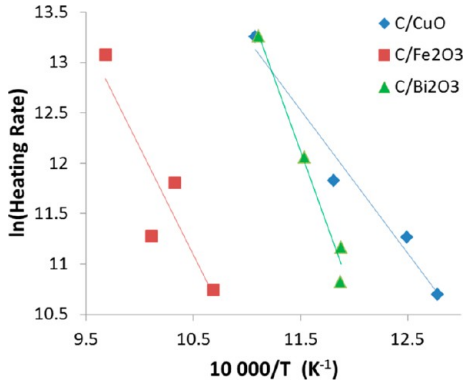

Figure 6. Arrhenius plots for the Ozawa isoconversion method. Each point is an averaged value from four experimental runs.

Table 2. Estimated Reaction Rates Using the NSC Model and Experimentally Determined Parameters

sample	temperature (K)	NSC reaction rate (g cm^{-2} s^{-1})	measured reaction rate (g cm^{-2} s^{-1})
C/Fe_2O_3	1020	5.6×10^{-7}	7×10^{-3}
C/Bi_2O_3	930	1.1×10^{-7}	2×10^{-2}
C/CuO	950	1.6×10^{-7}	1×10^{-2}
C/CuO	1210	7.7×10^{-6}	

endothermic reaction if reaction (1) is followed, the temperature of the wire is likely the highest possible temperature that oxidation takes place within this experiment. However, there is the possibility of self-heating during the exothermic C/CuO reaction. An estimated reaction temperature from CHEETAH 4.0[26] equilibrium code (at constant volume) for stoichiometric C/CuO, yields a temperature of 1210 K. This value is ~200 K higher than the initiation temperature of C/CuO of 1010 K. The estimate from the NSC model for this elevated temperature is listed in Table 2 and is an order of magnitude higher at 1209 K, but is still ~3 orders of magnitude lower than the experimentally predicted reaction rate.

The pressure for this system is difficult to assess. The experiments are performed under high vacuum conditions at 10^{-9} atm, but the reactions are also shown to proceed without the presence of a gas phase oxidizer. Due to the condensed nature of the reaction it is challenging to predict an effective partial pressure for use in the model. Fortunately, the reaction rate is only lightly dependent on pressure. We have previously estimated the concentration of O_2 within a sample volume of fuel/metal oxide nanoparticles to be ~55 kg m^{-13} [9] after complete release of the O_2 by the metal oxide. This value was used to determine the partial pressure of O_2 for each mixture at the temperatures given in Table 2.

A variable heating rate experiment was also performed to determine the apparent activation energy of the carbon oxidation process in each system. The temperature for the onset of CO_2 release for each system at several heating rates is given in Figure 5. Each point is an average of four experimental runs, and the error bars represent the standard deviation. The Osawa method[23,24] can be used to determine the activation energy from the slope of the Arrhenius plots in Figure 6. Initiation temperatures are in the range of 900 to 780 K for C/CuO, 1030 to 940 K for C/Fe_2O_3, and 900 to 840 K for C/Bi_2O_3 producing activation energies of 110 ± 12, 170 ± 27, and 230 ± 29 kJ mol^{-1}, respectively. The error was determined using the standard error from similar unaveraged plots. We attribute the relatively large error to the speed at which the reaction is taking place. In traditional DSC or TGA experiments, slower reaction events are generally observed, and more easily characterized. These results are significantly lower than the activation energy at slow heating rates for CuO decomposition to produce a gaseous oxidizer

$$CuO\ (s) \leftrightarrow Cu_2O\ (s) + O_2\ (g) \quad (3)$$

of 322.2 kJ mol^{-1},[27] but are consistent with the activation energy of O_2 release from CuO in recent high heating rate experiments of 132 kJ mol^{-1}.[28] Although the activation energy for the initiation of the fuel/metal oxide reaction is consistent with the gaseous O_2 release process at high heating rates, it does not necessarily mean that gas phase O_2 is required for initiation.

A slow heating-rate TEM study was also performed on C/CuO to observe the effect of low temperatures on the system. Figure 7a,b is the before and after images for heating at 500 K min^{-1} to 723 K. At this low temperature the extent of reaction is inconclusive, but it is clear that the CuO undergoes significant morphological changes despite the temperature being well below the bulk melting point of CuO at 1473 K. Siriwardane et al. observed similar changes for microscale C/CuO at 873 K.[7] These studies clearly show the mobility of metal oxides at temperatures well below their bulk melting points, and more in line with their Tammann temperatures (Tammann temperature for CuO is ~737 K). The ability of the metal oxide to become mobile and increase the effective surface area between fuel and oxidizer at low temperatures could be a key component of the initiation mechanism.

The occurrence of reaction without gaseous O_2 in the C/CuO and C/Fe_2O_3 systems clearly demonstrates the ability of these metal oxides to oxidize a fuel through the condensed state. In our previous T-Jump/TOFMS experiments with nanothermites, data showed that the ignition occurred for Al/CuO and Al/Fe_2O_3 at the point of gaseous O_2 release from the oxidizer.[9] More recent studies with nanothermites show that a condensed phase reactive sintering mechanism is responsible for initiation of these nanothermite reactions rather than a heterogeneous reaction between gaseous O_2 and aluminum.[11,14] Evidence to support this condensed state reaction has also been demonstrated for Al/Bi_2O_3 and C/Bi_2O_3.[10] The current results for carbon/metal oxides show similar characteristics to the reactive sintering process observed for aluminum nanothermites, but due to the difference in fuels (carbon and

dx.doi.org/10.1021/jp304148c | J. Phys. Chem. C 2012, 116, 24496−24502

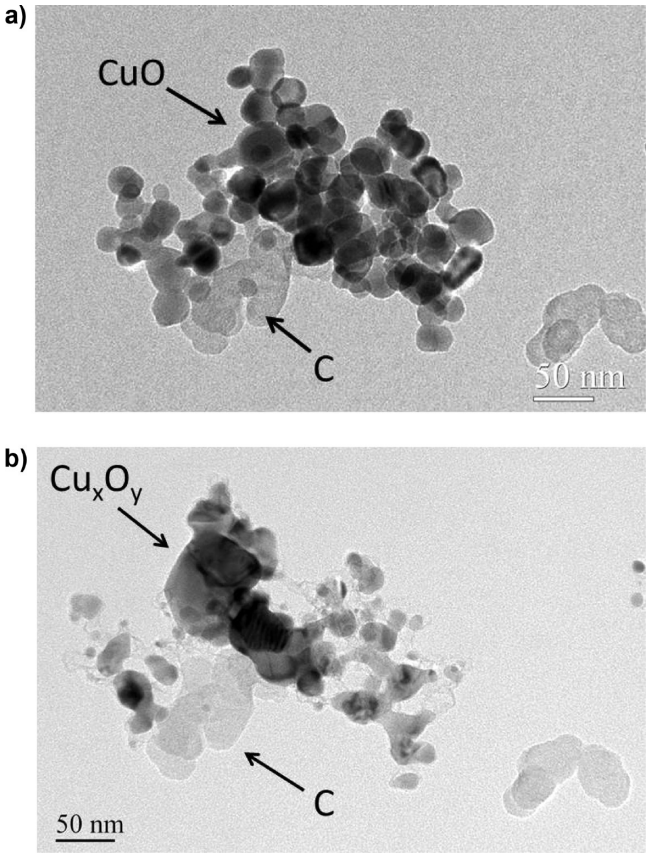

Figure 7. (a) TEM image of carbon and CuO nanoparticles prior to in situ heating. (b) TEM image of the resulting formation of the carbon/CuO particles in panel a, after in situ heating. Samples were heated at ~500 K/min, up to 723 K.

aluminum) there should be some variations in the reaction process. Unlike aluminum, carbon will remain in the solid phase and will not melt during the temperature regime of this study. Therefore carbon may not participate in the sintering process, but the metal oxide particles will, even without the aid of an exothermic reaction. This still allows for a more intimate contact between the carbon and metal oxide particles, and for C/CuO an exothermic reaction can further promote heating and sintering of the metal oxide. The TEM images in Figure 7a,b support this as considerable sintering is observed for the C/CuO reaction well below the melting point of CuO. Thus far we have argued that in the current study, the initiation of carbon oxidation is largely dependent on the ability of the metal oxide to oxidize the fuel in the condensed state. Therefore the choice of metal oxide will affect many aspects of the reaction including the initiation temperature. We have noted the mechanistic similarities between a mixture of carbon and metal oxide nanoparticles with a nanothermite, mainly that early sintering of the metal oxides helps to initiate condensed phase reaction and expand the effective reaction zone. Considering the same oxidizers have been investigated for both carbon and aluminum fuels, and initiation of the reaction is suggested to be dependent on the oxidizer, it is expected that reactions would proceed at the same temperature for each respective oxidizer. Table 3 highlights the initial reaction temperature for CuO and Fe_2O_3 with both carbon and aluminum as fuels, and shows that this is not the case as the aluminum systems ignite at higher temperatures.

Table 3. Initial Reaction Temperatures for CuO and Fe_2O_3 Mixed with Carbon or Aluminum at Heating Rates of 10^5 K s^{-1}

system	initial reaction temperature (K)	system	initial reaction temperature (K)
C/CuO	900	Al/CuO	1010[14]
C/Fe_2O_3	1030	Al/Fe_2O_3	1270[14]

This can be explained by the difference in the two fuels as aluminum is surrounded by the relatively inert Al_2O_3 shell while carbon does not have a protective shell. Once there is an oxidizing agent present for carbon, the fuel and oxidizer readily react. However for an aluminum fuel, once the oxidizer is present it is likely still separated from the aluminum metal by the Al_2O_3. Therefore, there will be some delay before the oxidizer and fuel come into contact. In a previous study we have seen the presence of ignition delays in nanothermites due to longer diffusion times from increased Al_2O_3 shell thickness. These delays were as large as ~2 ms for a 4 nm Al_2O_3 shell. In the present study we predict that during rapid heating, C/CuO reacts ~0.5 ms earlier than Al/CuO, and C/Fe_2O_3 reacts ~1.25 ms earlier than Al/Fe_2O_3. This is based on the time difference from CO_2 release in the carbon/metal oxide and the release of O_2 from the neat metal oxide as observed in Figures 2 and 3 (Al/CuO and Al/Fe_2O_3 ignite at the same temperature as gaseous O_2 is released). The delay time is consistent with the diffusion delay through the Al_2O_3 shell and complements the evidence for condensed phase reaction. Furthermore, the difference in delay for CuO and Fe_2O_3 further stresses that the ability of the oxide to transport oxygen in the condensed phase may play a large role in the speed of diffusion and hence the initiation process.

■ CONCLUSIONS

We have investigated the reaction of carbon/metal oxide mixtures using T-Jump/TOFMS. To determine the order of reaction events, the fuel/oxidizer as well as the neat nanopowders were separately sampled. Through the use of similar heating pulses,, comparison could be made between the timing of oxidizer release from the neat metal oxides and the reaction of carbon/metal oxide mixtures. During initiation of both C/CuO and C/Fe_2O_3, CO_2 was the first gaseous reaction product that appeared. This initiation event clearly occurred before the gaseous O_2 production by neat metal oxides. Without the presence of a gaseous oxidizer at the point of initiation, it is concluded that the initiation of the carbon combustion is due to a condensed phase reaction. Comparison with the NSC model suggests that the condensed phase reaction occurs at a much faster rate than traditional gas/solid heterogeneous reactions. Comparison of these findings for carbon oxidation with that of our previous aluminum nanothermite work shows significant similarities. In both the Al/WO_3 high heating rate SEM and the T-Jump X-ray imaging studies, there was significant evidence for a reactive sintering mechanism. The findings in the present study provide further evidence for this mechanism. There is a significant difference in the reaction temperature of carbon/metal oxides and aluminum/metal oxides despite similar initial reaction steps. We attribute the apparent higher reaction temperature of aluminum/metal oxide mixtures to a diffusion delay in aluminum combustion that is not present for carbon due to coating differences of the two fuels.

dx.doi.org/10.1021/jp304148c | J. Phys. Chem. C 2012, 116, 24496−24502

APPENDIX A

The NSC model[16]

$$\frac{w}{12} = \left(\frac{k_A P_{O_2}}{1 + k_z P_{O_2}}\right)\chi + k_B P_{O_2}(1 - \chi) \quad (1)$$

$$\chi = \left[1 + \frac{k_T}{k_B P_{O_2}}\right]^{-1} \quad (2)$$

$$k_A = 20 \exp\left(\frac{-15\,100}{T}\right) \quad (3)$$

$$k_B = 4.46 \times 10^{-3} \exp\left(\frac{-7640}{T}\right) \quad (4)$$

$$k_T = 1.51 \times 10^{5} \exp\left(\frac{-48\,800}{T}\right) \quad (5)$$

$$k_z = 21.3 \exp\left(\frac{2060}{T}\right) \quad (6)$$

where w is the specific reaction rate (kg $m^{-2}s^{-1}$), P_{O_2} is the partial pressure of O_2, and T is the temperature at the onset of reaction. The parameter values for a sample calculation for C/Fe_2O_3 are given in Table A1.

Table A1. Sample Parameters for the C/Fe_2O_3 System Used to Determine the Reaction Rate of Carbon at 1020 K

parameter for NSC model	value
T	1020 K
P_{O_2}	0.21 atm
k_A	7.4×10^{-6} g cm^{-2} s^{-1} atm^{-1}
k_B	2.5×10^{-6} g cm^{-2} s^{-1} atm^{-1}
k_T	2.5×10^{-16} g cm^{-2} s^{-1}
k_z	161 atm^{-1}
χ	1
w	5.4×10^{-7} g cm^{-2} s^{-1}

AUTHOR INFORMATION

Corresponding Author

*E-mail: mrz@umd.edu. Phone: 301-405-4311. Fax: 301-314-9477.

Notes

The authors declare no competing financial interest.

ACKNOWLEDGMENTS

This work was supported by the Army Research Office and the National Energy Technology Laboratory. The authors also acknowledge support from the University of Maryland Center for Energetic Concepts Development. We acknowledge the support of the Maryland NanoCenter and its NispLab. The NispLab is supported in part by the NSF as a MRSEC Shared Experimental Facility.

REFERENCES

(1) Richter, H. J.; Knoche, K. F. *ACS Symp. Ser.* **1983**, *235*, 71−85.
(2) Chuang, S. Y.; Dennis, J. S.; Hayhurst, A. N.; Scott, S. A. *Combust. Flame* **2008**, *154*, 109−121.
(3) Shen, L. H.; Wu, J. H.; Xiao, J.; Song, Q. L.; Xiao, R. *Energy Fuels* **2009**, *23*, 2498−2505.
(4) Scott, S. A.; Dennis, J. S.; Hayhurst, A. N.; Brown, T. *AlChE J.* **2006**, *52*, 3325−3328.
(5) Kronberger, B.; Lyngfelt, A.; Loffler, G.; Hofbauer, H. *Ind. Eng. Chem. Res.* **2005**, *44*, 546−556.
(6) Mattisson, T.; Lyngfelt, A.; Leion, H. *Int. J. Greenhouse Gas Control* **2009**, *3*, 11−19.
(7) Siriwardane, R.; Tian, H. J.; Miller, D.; Richards, G.; Simonyi, T.; Poston, J. *Combust. Flame* **2010**, *157*, 2198−2208.
(8) Satterfield, C. N. *Heterogeneous catalysis in industrial practice*. 2nd ed.; McGraw-Hill: New York, NY, 1991.
(9) Zhou, L.; Piekiel, N.; Chowdhury, S.; Zachariah, M. R. *J. Phys. Chem. C* **2010**, *114*, 14269−14275.
(10) Piekiel, N.; Zhou, L.; Sullivan, K.; Zachariah, M. R. *Combust. Sci. Technol.* submitted.
(11) Sullivan, K. T.; Chiou, W. A.; Fiore, R.; Zachariah, M. R. *Appl. Phys. Lett.* **2010**, *97*, 133104−133106.
(12) Shuk, P.; Wiemhofer, H. D.; Guth, U.; Gopel, W.; Greenblatt, M. *Solid State Ionics* **1996**, *89*, 179−196.
(13) Ermoline, A.; Stamatis, D.; Dreizin, E. L. *Thermochim. Acta* **2012**, 52−58.
(14) Sullivan, K. T.; Piekiel, N. W.; Wu, C.; Chowdhury, S.; Kelly, S. T.; Hufnagel, T. C.; Fezzaa, K.; Zachariah, M. R. *Combust. Flame* **2012**, *159*, 2−15.
(15) Brandt, O.; Roth, P. *Combust. Flame* **1989**, *77*, 69−78.
(16) Park, C.; Appleton, J. P. *Combust. Flame* **1973**, *20*, 369−379.
(17) Gilot, P.; Bonnefoy, F.; Marcuccilli, F.; Prado, G. *Combust. Flame* **1993**, *95*, 87−100.
(18) Walls, J. R.; Strickland-Constable, R. F. *Carbon* **1964**, *1*, 333−338.
(19) Neeft, J. P. A.; Nijhuis, T. X.; Smakman, E.; Makkee, M.; Moulijn, J. A. *Fuel* **1997**, *76*, 1129−1136.
(20) Higgins, K. J.; Jung, H. J.; Kittelson, D. B.; Roberts, J. T.; Zachariah, M. R. *J. Phys. Chem. A* **2002**, *106*, 96−103.
(21) Zhou, L.; Piekiel, N.; Chowdhury, S.; Zachariah, M. R. *Rapid Commun. Mass Spectrom.* **2009**, *23*, 194−202.
(22) Van Dusen, M. S. *J. Am. Chem. Soc.* **1925**, *47*, 326−332.
(23) Ozawa, T. *Bull. Chem. Soc. Jpn.* **1965**, *38*, 1881−1886.
(24) Vyazovkin, S.; Sbirrazzuoli, N. *Macromol. Rapid Commun.* **2006**, *27*, 1515−1532.
(25) Mikaia, A.; Zaikin, V.; Little, J.; Zhu, D.; Clifton, C.; Sparkman, D. *NIST/EPA/NIH Mass Spectral Library*; The Standard Reference Data Program; National Institute of Standards and Technology: Gaithersburg, MD, 2005.
(26) Fried, L. E.; Glaesemann, K. R.; Howard, W. M.; Souers, P. C.; Vitello, P. A. CHEETAH 4.0, Lawrence Livermore National Laboratory: Livermore, CA, 2004.
(27) Chadda, D.; Ford, J. D.; Fahim, M. A. *Int. J. Energ. Res.* **1989**, *13*, 63−73.
(28) Jian, G.; Zhou, L.; Piekiel, N. W.; Zachariah, M. R. Probing Oxygen Release Kinetics of Nanosized Metal Oxides by Temperature-Jump Time of Flight Mass Spectrometry. *Fall Technical Meeting of the Eastern States Section of the Combustion Institute*, The Combustion Institute: Pittsburgh, PA, 2011.